First-principles investigation of electronic, structural, and vibrational properties of a-Si_3N_4

Luigi Giacomazzi[1] and P. Umari[2]

[1]*CNR-INFM/Democritos National Simulation Center and the Abdus Salam International Centre for Theoretical Physics (ICTP), Strada Costiera 11, I-34151 Trieste, Italy*

[2]*CNR-INFM/Democritos National Simulation Center, Theory@Elettra Group, Area Science Park, Basovizza, I-34012 Trieste, Italy*

(Received 5 June 2009; revised manuscript received 23 September 2009; published 19 October 2009)

Using a density-functional scheme, we investigate the electronic, structural, and vibrational properties of amorphous silicon nitride. Through a Car-Parrinello molecular-dynamics simulation, we generate a model structure formed mainly by a network of SiN_4 tetrahedra a large fraction of which are edge sharing. Only a small fraction of atoms are overcoordinated and undercoordinated. First, the structural properties such as angular distributions, atomic arrangements in first-neighbor shells, the neutron total structure factor, the radial distribution function, and pair-correlation functions are examined. Next, the electronic properties are analyzed by considering the quasiparticle density of states which is calculated through the *GW* method. Good agreement is found with experimental data when available. Successively, we focus on a range of vibrational spectra. First, the vibrational density of states is analyzed in terms of its decomposition into N and Si contributions. Then, we investigate the Born effective charge tensors, the high-frequency, and static dielectric constants and calculate the real and imaginary parts of the dielectric function in the infrared. Therefrom we obtain the infrared-absorption spectrum and the refractive index that are found to be in accord with experimental measurements. Moreover, we address the Raman spectrum which is compared with available experimental data. Electronic structure and vibrational properties of the point defects present in our model are also discussed. Density-functional and *GW* schemes appear to be appropriate for modeling materials based on silicon nitride. In particular, our modeling of silicon nitride achieved a successful level of comparison with experiments. This allows us to infer that a-Si_3N_4 features a high content of edge-sharing tetrahedra, which are absent in the crystalline phases of silicon nitride at ambient conditions.

DOI: 10.1103/PhysRevB.80.144201 PACS number(s): 63.50.Lm, 78.30.−j, 61.43.Fs, 71.15.Mb

I. INTRODUCTION

Silicon nitride (Si_3N_4) is used in several fields of materials engineering where its mechanical and electronic properties lead to a wide range of applications.[1] In mechanical engineering, it is used as a material for cutting tools and engine parts. In microelectronics, amorphous silicon nitride (a-Si_3N_4) is used to fabricate insulating layers in triple oxide-nitride-oxide structures.[2] In particular, because of its high concentration of charge traps, a-Si_3N_4 is employed as charge storage layer in nonvolatile memory devices.[3] Moreover, silicon nitride based materials are nowadays proposed for optoelectronic devices.[4] Thin films of a-Si_3N_4 are grown either through chemical-vapor deposition (CVD) (Ref. 5) of silane and ammonia gases or through physical-vapor deposition (PVD).[6] Films obtained through CVD can contain a non-negligible fraction of hydrogen as deduced by the intensity of infrared-absorption peaks corresponding to the Si-H and N-H stretching modes around 2220 and 3300 cm^{-1}, respectively.[7–9] On the contrary, PVD techniques can give films with extremely low or no-hydrogen content. Yet, thin films produced by PVD techniques, e.g., by sputtering,[10] are usually affected by the presence of inhomogeneities. Thus growing high-purity and high quality thin films results of difficult control within both deposition techniques.

In a-Si_3N_4 silicon atoms are fourfold coordinated forming regular SiN_4 tetrahedra. The latter are connected by corners in such a way that each N atom is shared by three tetrahedra. Nitrogen atoms are threefold coordinated, with the silicon neighbors arranged at the vertices of a planar triangle. This results in a quite rigid network structure. Furthermore the a-Si_3N_4 network is supposed to contain not only corner sharing but also edge-sharing SiN_4 tetrahedra.[11] This structural picture mainly stems from the analysis of neutron and x-ray diffraction data.[12,13] However the knowledge which can be easily obtained from these experiments is limited to the atomic arrangements in the first- and second-nearest-neighbor shells.[14] Electronic spectra, such as the direct and inverse photoemission, and vibrational spectra, such as infrared and Raman permit to access a larger range of properties. However, the interpretation of the electronic and vibrational spectra is usually nontrivial and requires accurate modeling.[15–18] During the last decade, first-principles methods based on density-functional theory (DFT) (Ref. 19), and its extensions to excited states[20] have become extremely valuable tools for the investigation of the electronic and vibrational spectra of amorphous materials. Indeed, it is now possible to calculate from first principles a wide range of spectra for model structures which can be generated also through first-principles molecular-dynamics approaches. First-principles spectroscopy has been successfully applied to the study of amorphous SiO_2, GeO_2, $GeSe_2$, and B_2O_3.[14,21–23]

Although the structure of a-Si_3N_4 has been already modeled through classical potentials[24–27] and density-functional schemes,[11,28–31] computational spectroscopy investigations that model extended sets of experimental spectra are still lacking. Here, we provide a thorough analysis of a-Si_3N_4 based on first-principles spectroscopy. Our goal is twofold: first, we want to check the reliability of first-principles density-functional methods for the simulation of structural,

electronic, and vibrational spectra. Second, having validated our approach, we provide an analysis of the calculated spectra in terms of microscopic contributions. Through Car-Parrinello molecular dynamics we generate a model structure of a-Si_3N_4 showing high topological and chemical order. A structural analysis of our model shows that more than 90% of the Si atoms belong to regular tetrahedral units. Correspondingly, the largest part of N atoms show threefold coordination. Then, we calculate the neutron structure factor, the electronic and vibrational densities of states, the infrared and Raman spectra. The electronic density of states (DOS) is calculated through the *GW* approximation[32–34] of the many-body perturbation theory framework.[35] An overall good agreement is found with experimental data when available. Furthermore, the presence of undercoordinated and overcoordinated atoms in our model structure allows us to address structural, electronic, and vibrational properties of typical point defects found in experimental samples. We conclude that a-Si_3N_4 consists of a network of almost equivalent amounts of corner- and edge-sharing SiN_4 tetrahedra, together with a small fraction of Si and N atoms overcoordinated or undercoordinated.

This paper is organized as follows. In Sec. II, we describe the generation of our model structure of a-Si_3N_4, and we report the technical details of our electronic-structure calculations. In Sec. III, we address the structural properties of a-Si_3N_4. In particular, we report bond-length and bond-angle distributions, the neutron total structure factor, the radial distribution function (RDF) and the pair-correlation functions (PCFs). In Sec. IV we give and analyze the electronic density of states of our model structure which is calculated through an accurate *GW* scheme. The electronic properties of the defects in our model structure are also discussed. The localization of the electronic states is then discussed through the inverse participation ratio. Section V is devoted to the vibrational density of states (v-DOS), which is analyzed in terms of Si and N contributions. Moreover, partial vibrational density of states of point defects are calculated and analyzed. Section VI focuses on infrared properties, such as the dynamical Born charges and the dielectric function. Then, the infrared-absorption spectrum and the refractive index are given and compared to experimental results. In Sec. VII, we address the Raman spectra. Finally, Sec. VIII contains the conclusions of our work.

II. MODEL GENERATION AND TECHNICAL DETAILS

A. Technical details

In the present work, we have performed first-principles electronic-structure calculations based on density-functional theory. For generating the model structure of a-Si_3N_4 we carried out molecular-dynamics simulations using the Car-Parrinello method.[36,37] In particular, we used the computational codes and pseudopotentials from the QUANTUM-ESPRESSO package.[38] The exchange and correlation functional was approximated through the local-density approximation (LDA).[39] Core-valence interactions were described through ultrasoft pseudopotentials[40] for N and H atoms and through a norm-conserving pseudopotential for Si atoms. The electronic wave functions and the charge density were expanded using plane-wave basis sets defined by energy cutoffs of 25 and 200 Ry, respectively. The Brillouin's zone was sampled at the Γ point. The electronic density of states was then calculated through a *GW* approach[41] based on the analytic continuation scheme which permits to overcome the simpler plasmon-pole approximation.[34] First, the polarization propagator basis was obtained including 750 conduction states and a cutoff $s_2=0.1$ a.u., then for calculating the quasiparticle energies we considered 1500 conduction states.[41] We derived the vibrational frequencies and eigenmodes by diagonalizing the dynamical matrix,[14] which we calculated numerically by taking finite differences of the atomic forces. To this purpose we used atomic displacements of 0.05 bohr. For accessing the infrared and Raman spectra, we took advantage from the finite electric field scheme.[18] Indeed, we obtained the relevant coupling tensors by numerically calculating first and second derivatives of the atomic forces with respect to the electric fields.[14,42] We applied fields of ± 0.002 a.u. We checked the convergence of the coupling tensors by considering an additional set of forces obtained by applying electric fields of ± 0.001 a.u. but found negligible modifications of the calculated spectra.

B. Model generation

The model was generated starting from a diamond-cubic model of crystalline silicon which was changed into Si_3N_4 by addition of N atoms at intermediate distances between Si–Si neighbors. The initial model structure contained 64 Si and 86 N atoms in a periodically repeated cubic cell. A composition ratio $r=[N]/[Si]$ of 1.34 was chosen slightly differing from the ideal stoichiometry in order to trigger the formation of defects. We set up the density to the experimental value of 3.1 g/cm^3.[43,44] Molecular dynamics runs were then performed for obtaining the model of a-Si_3N_4. First the system was thermalized at the temperature of 3500 K for 12 ps using a Nosé-Hoover thermostat.[45] Successively, the sample was quenched for 5 ps down to 2000 K below the theoretical melting point. Finally, the structural geometry was further optimized by a damped molecular-dynamics run. As the model presented an empty state close to the top of the valence band, we passivated it by adding to the structure two H atoms in proximity of the two Si atoms which were threefold coordinated.[30,46] After structural relaxation, the H atoms moved close to two near N sites. We note that the structural and electronic properties of our model were only marginally affected by the addition of the two H atoms. Snapshots of the final structure are given in Fig. 1.

III. STRUCTURAL PROPERTIES

A. Model structural analysis

We analyze the short range order of our model by considering bond-angle and bond-length distributions (Table I). The average Si-N bond length equals to 1.730 Å with a standard deviation (std) of 0.060 Å. This value is found in excellent agreement with the experimental bond length of 1.729 Å.[12] In Fig. 2(a), we display the Si-N bond-length distribution.

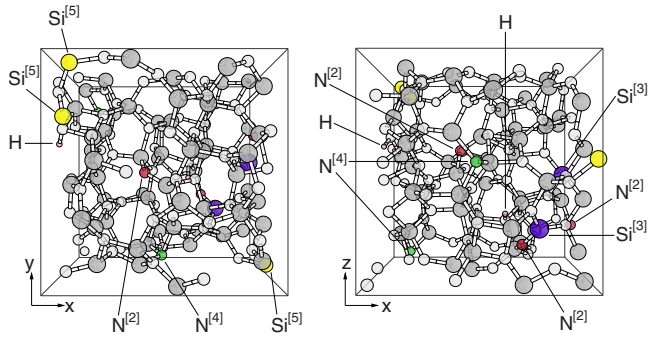

FIG. 1. (Color online) Snapshots of the a-Si_3N_4 model. Si atoms and N atoms are colored with dark and light gray, respectively. Threefold and fivefold coordinated Si atoms are colored in purple and yellow, respectively. Twofold and fourfold coordinated N atoms are colored in red and green. Hydrogen are colored in pink. Defect atoms are also labeled according to the text.

This shows a peak at ~1.73 Å with a width close to those registered in other amorphous materials[21] and slightly wider than that found for the Si-O bond length in silica.[14] The two H atoms present in our model are bonded with N atoms with bond lengths of 1.03 and 1.04 Å.

Our model structure shows well defined SiN_4 tetrahedral units. As we can see from the distribution of the N-Si-N angle, which is reported in Fig. 2(b), the average N-Si-N angle equals 109.1° with a standard deviation of 13°. This is very close to the ideal angle of 109.47° for regular tetrahedra. Moreover our structure shows also well defined quasiplanar NSi_3 units. We give in Fig. 2(b) the Si-N-Si bond-angle distribution: the average Si-N-Si angle equals 117.2° with a standard deviation of 15°. This is consistent with the value of 120° for regular planar NSi_3 units. The amount of SiN_4 tetrahedra and NSi_3 triangular units is reported in Table II where we give the coordination numbers in the first-neighbor shells of Si and N atoms, together with the relative Si-N bond length averages. The majority of Si atoms is fourfold coordinated and shows an average Si-N bond length of 1.73 Å. Few Si atoms are threefold or fivefold coordinated. Correspondingly, almost all nitrogen atoms are bound to three silicon and only a few show twofold or fourfold coordination. Consequently, our model shows at short-range high topological and chemical order. The presence of N atoms twofold coordinated ($N^{[2]}$) and Si atoms threefold coordinated ($Si^{[3]}$) in silicon nitride samples is experimentally established by means of electron-paramagnetic resonance.[47] Moreover, these types of defects have been the object of past

TABLE I. Structural properties of our model of a-Si_3N_4 and reference values: average Si-N-Si and N-Si-N angles and average bond length d_{SiN}. The respective standard deviations are given in parenthesis.

	∠Si-N-Si	∠N-Si-N	d_{SiN}(Å)
Model	117.2° (15.1°)	109.1° (13.0°)	1.73 (0.06)
Ref.	120° [a]	109.47° [a]	1.729[b]

[a]Ideal bonding geometry.
[b]Experiment (Ref. 12).

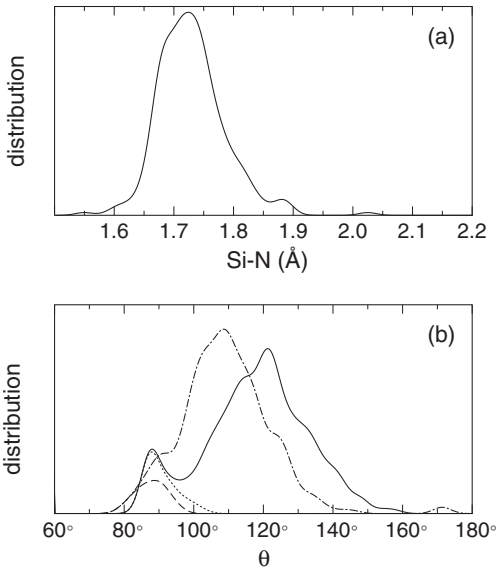

FIG. 2. (a) Distribution of Si-N bond lengths. A Gaussian broadening of 0.015 Å is used. (b) Distributions of the Si-N-Si (solid) and N-Si-N angles (dot dashed). Contributions from angles Si-N-Si and N-Si-N in twofold rings are shown (dotted and dashed, respectively). Normalization to unity and a Gaussian broadening of 2.5° are used.

investigations which demonstrated that they can act as deep electron traps.[31] Experimental estimates of the concentration of twofold coordinated N and threefold coordinated Si range between 10^{17} up to 10^{20} cm^{-3}.[48] *Ab initio* calculations with supercells of a size large enough for having realistic concentrations of these defects are currently not affordable. Hence, *ab initio* simulations currently lead to overestimating the experimental concentrations. In our model only few coordination defects are present and thus the actual overestimation is as low as feasible.

Though there is no direct experimental evidence of fivefold coordinated Si atoms ($Si^{[5]}$) in silicon nitride, several experimental works have found $Si^{[5]}$ atoms in silicate glasses.[49] We are not aware of experimental evidence of fourfold coordinated N atoms ($N^{[4]}$). The concentrations of coordination defects in our model might be affected by the delocalization issue of standard DFT.[50] However, it is not yet clear if more advanced DFT approaches such as hybrid functionals or self-interaction correction (SIC) methods would avoid the presence of overcoordination defects. The use of hybrid functionals or SIC could improve the description of the electronic properties of defects states,[51] but their computational cost prevents to use them for the long molecular-dynamics simulations necessaries for quenching a liquid, especially for large systems. Moreover, though SIC is known to work for treating an unpaired electron or hole,[52] none general and reliable SIC scheme has been developed so far.[53]

$N^{[2]}$ and $Si^{[3]}$ atoms in our model structure form bonds that are considerably shorter than the model average.[54] Indeed, for the $N^{[2]}$ atoms, we register an average bond length N-Si equal to 1.61 Å, while for the $Si^{[3]}$ atoms, we register an average Si-N equal to 1.64 Å. N atoms fourfold coordinated and Si atoms fivefold coordinated show a Si–N bond

TABLE II. Composition of first-neighbor shells in our model of a-Si_3N_4. Coordination numbers of Si and N atoms are indicated by the superscript number in square brackets. The number of Si and N atoms found in our model for each coordination are indicated by n_{Si} and n_N. Average Si-N bond length d_{SiN} (Å) together with its standard deviation (in parenthesis) is given for each composition. We used cut-off radii of 2.2 Å,

Composition	n_{Si}	d_{SiN}	Composition	n_N	d_{SiN}
$Si^{[3]}$	2	1.64(0.05)	$N^{[2]}$	3	1.61(0.03)
$Si^{[4]}$	59	1.73(0.05)	$N^{[3]}$	79	1.73(0.05)
$Si^{[5]}$	3	1.81(0.09)	$N^{[4]}$	2	1.85(0.09)
			NSi_3H	2	1.78(0.02)

length larger that the model average (Table II). The Si–N bond lengths of the two N atoms having a H neighbor are only slightly larger than the model average, suggesting that hydrogen is just weakly affecting the Si-N bonds.

The Si-N-Si angle distribution [Fig. 2(b)] can give also insight into the organization of the structural network beyond short range. Indeed, beside the main peak, the Si-N-Si angle distribution features a distinct peak at about 90°. This peak is due to edge-sharing tetrahedra. Indeed an atomic configuration involving edge-sharing tetrahedra gives rise to a twofold ring in which Si and N atoms alternate at the vertexes of a square. We note that this type of ring was shown to constitute the main N defect in silicon[55] and might play an important role also in the silicon nitride network. Our model structure contains sixteen twofold rings. These are found to be quasiplanar, with an average sum of bond angles of 356.6° very close to the ideal value of 360° for the perfectly planar ring. In these rings, the average Si-N-Si angle amounts to 90.5° with a standard deviation of 4.3° consistently with the distribution depicted in Fig. 2(b). The Si-N bond length in twofold rings averages to 1.76 Å with a standard deviation of 0.08 Å, slightly larger than the average bond length calculated by excluding the twofold rings (1.73 Å). The crystalline phase β-Si_3N_4 is formed by a structural network containing three-, four-, and six-membered rings.[56] The phase α-Si_3N_4 whose primitive cell is larger than that of β-Si_3N_4 presents fivefold and sevenfold rings in addition.[56] Twofold rings can be traced only in the high-pressure crystalline phase.[57] At variance our model of a-Si_3N_4 features a noticeable fraction of edge-sharing tetrahedra and therefore of twofold rings. Indeed, in our model 39% of the silicon and 31% of the nitrogen atoms belong to twofold rings. Hence the presence of edge-sharing tetrahedra might constitute one of the main topological differences between a-Si_3N_4 and its crystalline counterparts at ambient conditions.

B. Neutron structure factor

For assessing the quality of our model structure we calculated the neutron structure factor at room temperature accounting for the vibrations in the harmonic approximation.[17] We adopted scattering lengths of 9.36 and 4.149 fm for N and Si, respectively.[58] For simplicity, in the following structural analysis we did not take into account the H atoms that are present in low concentration in our model. In Fig. 3, we compare the calculated neutron structure factor with experimental data.[12] We note an overall nice agreement meaning that our model describes well the structural properties of a-Si_3N_4.

We calculated the RDF and the PCFs using Gaussian correlations of which the spread is derived from vibrational eigenmodes and frequencies obtained in the harmonic approximation. A detailed account of this approach is given in Ref. 17. This formulation offers the advantage of accounting for the zero-point motion and has been found to give a good description of oxide glasses at 300 K.[59,60] Figure 4 shows the RDF calculated at room temperature compared to the neutron scattering data of Ref. 12. Overall, we register a good agreement between experiment and theory. In particular, the calculated and experimental RDF well agree in correspondence of the two main peaks at 1.73 and 2.81 Å. We notice in the experimental RDF the presence of a small feature at about 1.2 Å, which is absent in the calculated RDF. This feature might arise from the presence in the experimental samples of H atoms which have been neglected in the calculation.

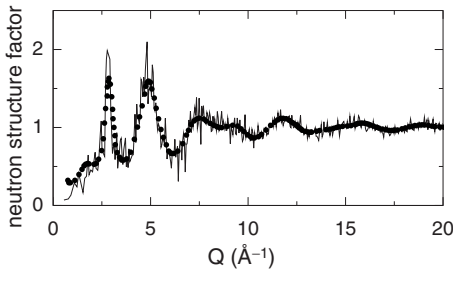

FIG. 3. Neutron structure factor at room temperature (solid) compared to the experimental data (circles) from Ref. 12.

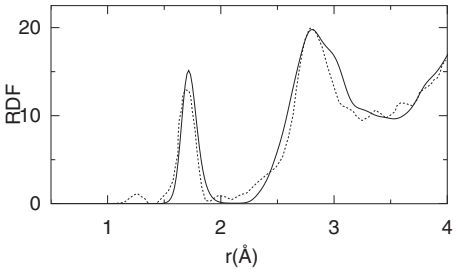

FIG. 4. Radial distribution function of a-Si_3N_4 calculated at room temperature (solid) and experimental data (dotted) from Ref. 12.

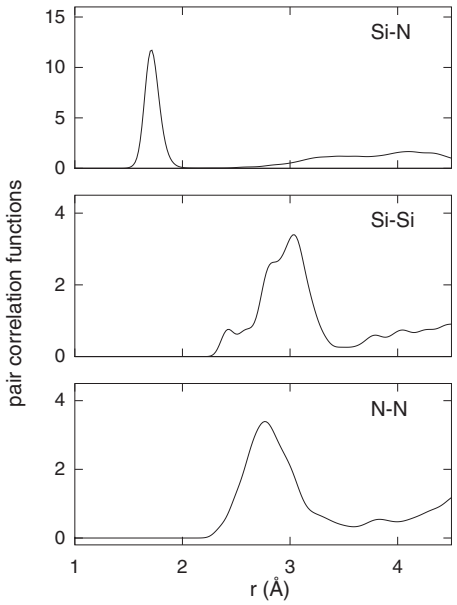

FIG. 5. Pair-correlation functions of a-Si_3N_4 calculated at room temperature (solid).

Figure 5 shows the PCFs calculated at room temperature for our model of a-Si_3N_4. The Si-N PCF is dominated by a strong peak in correspondence of the Si-N bond length, clearly corresponding to the first peak in Fig. 4. A spherical integration of the first peak in the Si-N PCF gives a coordination number of 4.02, consistently with the tetrahedral local environment of the Si first-neighbor shell. The main peak in the Si-Si PCF is located at 3.03 Å. The smaller peak at 2.42 Å is a fingerprint of the presence of edge-sharing tetrahedra. This together with the main peak, which stems from corner-sharing tetrahedra, reflects the Si-N-Si angle distribution [Fig. 2(b)]. We suggest that a higher content of edge-sharing tetrahedra might improve the agreement between calculated and experimental RDF around 2.4 Å (Fig. 4). The main peak in the N–N PCF is located at 2.76 Å. This gives origin to the second peak in the RDF at 2.81 Å. The small difference in position should be attributed to the contribution of the Si–Si PCF to the RDF.

IV. ELECTRONIC STRUCTURE

We show in Fig. 6(a) the electronic DOS for our model calculated with the *GW* approach together with the partial densities of *s* and *p* states for the Si and N atoms. The lowest part of the valence band mainly arises from N 2*s* states. While the low-energy side of the upper part of the valence band results from the Si-N bonds, formed by Si sp^3 and N 2*p* orbitals, the high-energy side, which defines the top of the valence band, consists of N 2*p* lone pairs. The low-energy side of the conduction band mainly consists of antibonding states associated to the Si-N bond. We note that the origin of the bands is analogous to the cases of SiO_2 (Ref. 61) and GeO_2 (Ref. 17), reflecting the common type of short-range arrangement of atoms based on the tetrahedral unit. Similar conclusions were obtained for electronic densities of states

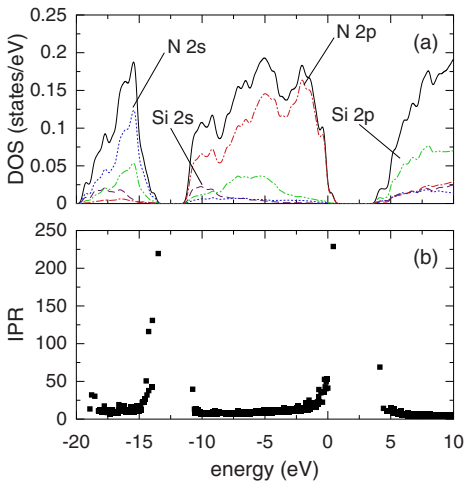

FIG. 6. (Color online) (a) Electronic density of states (black) and partial DOS obtained by projecting electronic states onto N 2*s* (blue/dotted), N 2*p* (red/dot-dashed), Si 2*s* (purple/dashed) and Si 2*p* (green/double dot-dashed). The highest occupied state is aligned at 0 eV. Gaussian broadening of 0.25 eV is used. *GW* energies are used. (b) Inverse participation ratio (IPR) of electronic states in silicon nitride.

calculated through an approximate density-functional scheme[62] and through a tight-binding approach.[63] Moreover, the calculated valence band is consistent with photoemission spectra.[64]

We focus now on the role played by the defects in the density of states. In Fig. 7(a) we give the partial DOS obtained by projecting the electronic states onto the 1*s* orbitals of the two H atoms of our model structure. The partial DOS of H atoms constitutes a very small contribution to the total DOS of Fig. 6. In Figs. 7(b) and 7(c) we show the partial DOS obtained by projecting the electronic states onto the 2*p* and 2*s* orbitals of the $N^{[2]}$ and $N^{[4]}$ atoms and of the $Si^{[3]}$ and $Si^{[5]}$ atoms. The partial DOS of $N^{[4]}$ atoms and $Si^{[5]}$ atoms do not show features localized near the band edges. At variance, the partial DOS of the $N^{[2]}$ atoms shows a sharp peak at the top of the valence band, while the partial DOS of $Si^{[3]}$ atoms exhibits sharp peaks close to the bottom of the conduction band.[65] As Fig. 7(a) illustrates, these peaks are originated by N and Si 2*p* orbitals of $N^{[2]}$ and $Si^{[3]}$ atoms, respectively. Furthermore, the topmost occupied electronic state and the first empty electronic state are spatially localized around a $N^{[2]}$ atom and around a $Si^{[3]}$ atom, respectively. By excluding these two defect states, we found a highest occupied molecular orbital–lowest unoccupied molecular orbital (HOMO-LUMO) band gap of 4.42 eV in excellent agreement with the experimental value of 4.55 eV of the optical band gap of sputtered a-Si_3N_4 given in Ref. 66. However, we note that the band gap is quite sensitive to the adopted production method and for CVD samples is about 5.3 eV.[66] Yet, the *GW* method appears to correctly describe the electronic density of states where simpler LDA calculations fail giving for our model structure a HOMO-LUMO band gap of only 2.9 eV, as typical for LDA calculations in silicon nitride.[30,62]

We now analyze the degree of localization of the electronic states. The localization of an electronic state can be

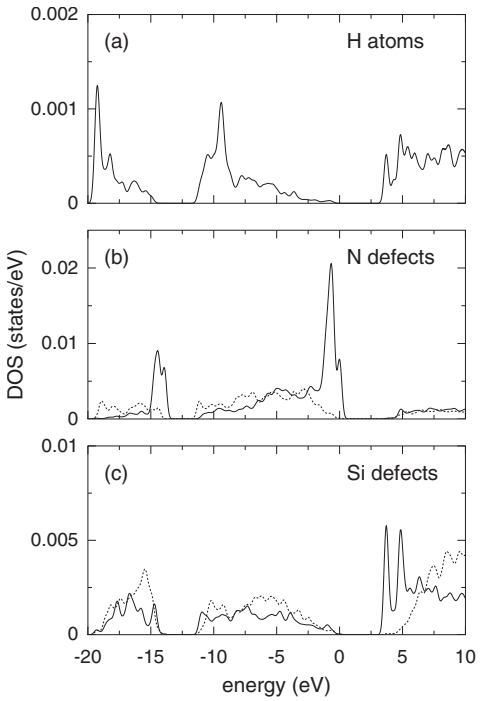

FIG. 7. Partial DOS obtained by projecting the electronic states onto (a) 1*s* orbitals of H atoms, (b) 2*p* and 2*s* orbitals of twofold (solid) and fourfold (dotted) coordinated N atoms, (c) 2*p* and 2*s* orbitals of threefold (solid) and fivefold (dotted) coordinated Si atoms. The highest occupied state is aligned at 0 eV. Gaussian broadening of 0.25 eV is used. *GW* energies are used.

quantified by the inverse participation ratio (IPR).[67] The larger the IPR the more localized is the electronic state so that highly localized or delocalized states show a large or small IPR. In Fig. 6(b) we show the IPRs for the electronic states of our model of silicon nitride. We note that the states close to the band edges corresponding to $N^{[2]}$ and $Si^{[3]}$ defects result much more localized than the other electronic states. These results are consistent with the IPR data previously calculated for a-SiN_x in Ref. 30.

V. VIBRATIONAL PROPERTIES

In Fig. 8(a), we display the calculated v-DOS for our model of silicon nitride together with its decomposition according to H, N, and Si contributions. While the low-frequency part of the spectrum, below ~550 cm^{-1}, stems equally from Si and N vibrations, the N character becomes dominant in the high-frequency part, above ~750 cm^{-1}. We note that the contribution from H atoms is almost negligible due to their low concentration and appears only above 1000 cm^{-1}. Although similar conclusions have been obtained through classical molecular-dynamics simulations,[27,68,69] our v-DOS differs at least in two aspects. First, the width of our spectrum is about a hundred cm^{-1} narrower than that reported in Ref. 27. Second, our v-DOS presents a peak at about 650 cm^{-1} which is absent in the classical molecular-dynamics results.[27] This peak is originated mainly from Si motions.

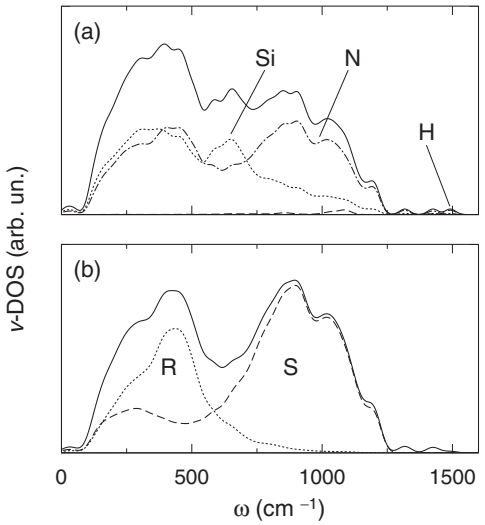

FIG. 8. (a) Vibrational density of states (v-DOS) of a-Si_3N_4 and its decomposition into Si (dotted), N (dot-dashed), and H (dashed) contributions. (b) Decomposition of the N contribution (solid) to the v-DOS into rocking motions out of the plane of Si neighbors (dotted) and into stretching motions in the plane of Si neighbors (dashed). (Only threefold coordinated N atoms are taken into account.) A Gaussian broadening of 25 cm^{-1} is used.

We further decomposed the nitrogen contribution to the v-DOS according to three orthogonal directions defining the local environment of the N atoms.[70] The first direction, which we refer as rocking, is taken orthogonal to the plane of the three Si neighbors. Then, the second one is taken along the bisector of one of the three Si-Si-Si angle and the third one is given by the cross product of the first two. The latter two directions define the stretching motion in the plane of the three Si neighbors. In Fig. 8(b) we show the partial v-DOS accounting for N vibrations along rocking and stretching directions. This decomposition shows that rocking motions and stretching motions give rise to well separate bands below and above 600 cm^{-1}. The contribution to the v-DOS due to rocking motions is maximal at about 440 cm^{-1}, while the contribution due to stretching motions totally accounts for the peak at ~900 cm^{-1}. In the crystalline phases α-Si_3N_4 and β-Si_3N_4 nitrogen vibrations in the range 300–500 cm^{-1} and above 800 cm^{-1} have been recently ascribed to bond bending (rocking) in NSi_3 triangles and to bond stretching, respectively.[71] Our analysis of the nitrogen motion in amorphous silicon nitride agrees with this assignment.

In order to understand how the point defects present in our model structure (Table II) may affect the vibrational spectra, we focus on the contribution to the v-DOS coming from single atoms.[70] In Fig. 9(a) we show the partial v-DOS of the two H atoms of our model structure. The highest frequency peaks at ~3300 cm^{-1} arise from the stretching motion of the N-H bonds. The peaks at 657, 855, ~1060, and 1487 cm^{-1} are related to motions of the hydrogen atoms in the plane normal to the N-H bond. Furthermore, we note that the frequencies of the three highest-frequency peaks at ~1060, 1487, and ~3300 cm^{-1} in Fig. 9(a) are in good agreement with the experimental infrared-absorption results

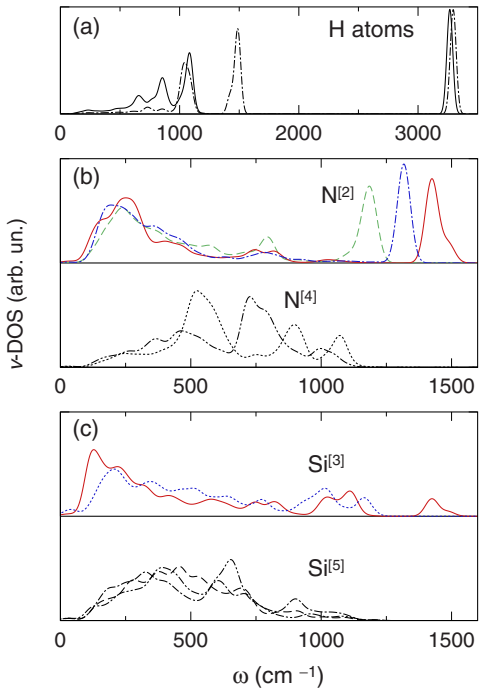

FIG. 9. (Color online) (a) Contributions to the v-DOS of each H atom in our model. (b) Contributions to the v-DOS of each twofold coordinated (upper panel) and fourfold coordinated N atom (lower panel) (c) Contributions to the v-DOS of each threefold (upper panel) and fivefold coordinated Si atom (lower panel). A Gaussian broadening of 25 cm^{-1} is used.

of Ref. 72. In Fig. 9(b) we give the partial v-DOS for each $N^{[2]}$ and $N^{[4]}$ atom in our model structure. $N^{[2]}$ atoms give peaks at ~250, ~800 cm^{-1}, and three main peaks at 1185, 1317, and 1425 cm^{-1}, thus differing noticeably from the behavior of the nitrogen partial v-DOS which becomes negligible above ~1200 cm^{-1} [Fig. 8(a)]. For each $N^{[2]}$ atom, we examined the nearest Si neighbor bond distances and found a trend between the position of the highest frequency peaks and the average Si-N bond distance. This is analogous to the dependency of the bond stretching frequencies from the bond length that is observed in silicon/oxides interfaces.[73] In particular we remark that the frequency peak at 1425 cm^{-1} is obtained for the $N^{[2]}$ atom featuring the shortest average of Si-N bonds (1.58 Å). The other two peaks at 1317 and 1185 cm^{-1} arise from stretching of bonds belonging to the other two $N^{[2]}$ atoms whose average Si-N bond lengths are 1.60 and 1.63 Å, respectively. The partial v-DOS of $N^{[4]}$ atoms gives main peaks at 524 and 727 cm^{-1}, but no intensity above 1200 cm^{-1}. We note that these peaks fall, respectively, at the right side of the rocking and at the left side of the stretching bands of the decomposition shown in Fig. 8(b). By contrast, we remark that the partial v-DOS of $N^{[2]}$ atoms gives the strongest peaks at the left side of the rocking and at the right side of the stretching bands.

In Fig. 9(c) we show the partial v-DOS for each $Si^{[3]}$ and $Si^{[5]}$ atom in our model structure. $Si^{[3]}$ atoms give main peaks at ~200 cm^{-1} and ~1000–1100 cm^{-1}. Thus contributions from $Si^{[3]}$ mainly appears at the right and left sides of the Si band shown in Fig. 8(a). We note that the peak at ~1425 cm^{-1} in Fig. 9(c) corresponds to the peak at the same frequency shown in Fig. 9(b). This is a consequence of the fact that the $N^{[2]}$ atom and the $Si^{[3]}$ atom under examination are nearest neighbors (Fig. 1). Hence they share the same bond stretching frequency. Finally, $Si^{[5]}$ atoms give contributions to the v-DOS markedly different from those pertaining to $Si^{[3]}$ atoms and more resembling the average behavior of Si atoms of Fig. 8. This indicates that $Si^{[5]}$ constitute only a weak perturbation for phonons in silicon nitride. The present analysis suggests that coordination defects in silicon nitride contribute to the vibrational density of states mainly at the edges of the rocking (250–550 cm^{-1}) and stretching (750–1250 cm^{-1}) vibrational bands. Similarly, we note that past investigations on amorphous silicon have shown that point defects contribute to the vibrational spectra at the sides of the main vibrational features.[74,75]

VI. INFRARED SPECTRA

A. Born charge tensors

We focus now on the dielectric properties in the infrared. The coupling between vibrational motions and the electric field can be described in terms of dynamical Born charge tensors.[76] Hence, we calculated Born charge tensors Z^* for Si and N atoms in our model. As the Si atoms have a predominant tetrahedral bonding configuration, the corresponding Born charge tensors are expected to show a strong isotropic character.[77] Averaging over the Si Z^*, we obtained[78]

$$Z^*_{\mathrm{Si}} = \begin{pmatrix} 3.28 & 0.07 & 0.02 \\ 0.07 & 3.33 & -0.03 \\ 0.01 & -0.03 & 3.36 \end{pmatrix}, \tag{1}$$

with a standard deviation of ~0.33 a.u. for each element in the matrix. Hence, the silicon Born charge tensors can be considered isotropic with a value of about 3.33 a.u.

This result is consistent with calculations for the crystalline phase β-Si_3N_4 in Ref. 77 yielding an isotropic Born charge of 3.38 a.u. Hydrogen atoms show an average Born charge of 0.39 a.u. This value is consistent with typical values of hydrogen Born charges reported in the literature.[79] Most of the N atoms are bonded, in a quasiplanar configuration, with three Si neighbors. This allows us to report their dynamical Born charge tensors with respect to a local reference system based on the orientation of the NSi_3 unit as done in Sec. V for decomposing the N contribution to the v-DOS. We take the x, y, and z directions along the bisector of a Si-Si-Si angle, the normal to the plane of the Si neighbors, and the normal to the two previous directions. By averaging over all the threefold coordinated N atoms ($N^{[3]}$) and for each atom over three possible choices for the Si-Si-Si bisector, we found (in a.u.)

$$Z^*_{\mathrm{N}} = \begin{pmatrix} -2.92 & 0.02 & -0.01 \\ 0.02 & -1.70 & -0.02 \\ 0.01 & -0.02 & -2.83 \end{pmatrix}, \tag{2}$$

with a standard deviation of ~0.20 a.u. for each element in the matrix. Hence, the average Z^*_{N} tensor is well described by

TABLE III. High-frequency (ϵ_∞) and static (ϵ_0) dielectric constants, calculated for our model of a-Si_3N_4. Experimental data are taken from Refs. 80 and 81.

	Model	Expt.
ϵ_∞	3.9	~4.2
ϵ_0	8.8	6–9

a diagonal tensor as already found for the oxygen atoms in silica and germania.[15,17] The smallest coupling to the electric field is found along the normal to the plane formed by the three Si neighbors, while the largest coupling is found for directions lying in the plane. We note that the isotropic average of the N Born-charge tensors yields −2.49 a.u. in accord with the value of −2.54 a.u. reported for the crystalline phase β-Si_3N_4 in Ref. 77.

We finally considered the average Born-charge tensor $Z^*_{N[2]}$ for the twofold coordinated N atoms and found (in a.u.)

$$Z^*_{N[2]} = \begin{pmatrix} -1.81 & 0.00 & -0.10 \\ 0.01 & -1.66 & -0.04 \\ -0.04 & 0.06 & -3.56 \end{pmatrix}, \quad (3)$$

where we have a standard deviation of ~0.1 a.u., and in order to compare with Eq. (2), we chose the following assignment: the first axis is taken along the Si-N-Si bisector, while the second axis corresponds to the perpendicular to the Si-N-Si plane, and the third one is given by the cross product of the first and second directions. We note that both the twofold and threefold coordinated N atoms show the same coupling in the direction normal to the Si-N-Si plane. The isotropic average of the Born-charge tensors for the $N^{[2]}$ atoms yields −2.34 a.u. slightly smaller than the average −2.49 a.u. $N^{[4]}$ atoms show an isotropic average Born charge of −2.60 a.u. larger than the global average −2.49 a.u. obtained for the $N^{[3]}$ atoms. Hence, the dynamical charge is found to decrease consistently with the increased number of Si neighbors. For the threefold coordinated Si atoms, we found an isotropic average Born charge of 3.24 a.u. slightly differing from the average for the $Si^{[4]}$ atoms (3.32 a.u.). Fivefold coordinated Si atoms show as expected a larger isotropic average Born charge: 3.53 a.u.

B. Infrared absorption spectrum

We consider for our model structure the high-frequency (ϵ_∞) and static (ϵ_0) dielectric constants. The first is obtained from the derivative, calculated by finite differences, of the induced polarization with respect to the electric field.[18,42] As given in Table III, we found, upon averaging, a value of ϵ_∞ =3.9, which is in fair accord with the value ϵ_∞=4.2 reported from experiments in amorphous silicon nitride.[80] We calculated the ϵ_0 by considering the vibrational frequencies and their corresponding oscillator strengths as illustrated in Refs. 14 and 15. The static dielectric constant of amorphous silicon nitride films can vary from 6 up to 9 depending on the film density and stoichiometry.[81] For instance, the static dielectric constant for a stoichiometric film at a density 2.7 g/cm^3 is

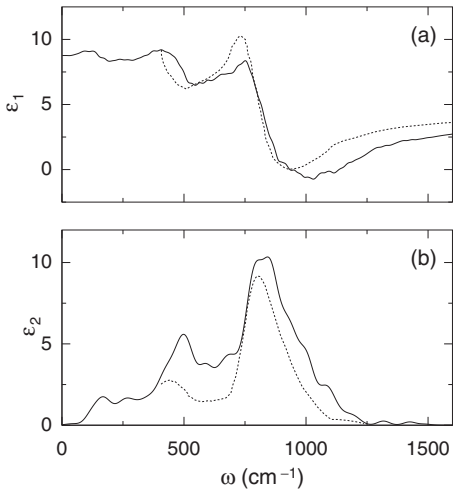

FIG. 10. Calculated (solid) (a) real and (b) imaginary parts of the dielectric function of a-Si_3N_4 in the infrared region compared to experimental results of Ref. 83 (dotted). A Lorentzian and a Gaussian broadening of 25 cm^{-1} are used.

~7.5 and tends to be higher in more Si-rich films.[82] The calculated static dielectric constant for our model structure has a value of ϵ_0=8.8. At the light of the above discussion, this value can be considered as in fair accord with the experimental literature.

The high-frequency dielectric constant, the vibrational frequencies, and their corresponding oscillator strengths fully determine the dielectric function in the infrared.[15,17] In Fig. 10, we compare the real (ϵ_1) and imaginary (ϵ_2) parts of the dielectric function calculated for our model of a-Si_3N_4 with experimental results.[83] The ϵ_2 features two broad peaks at about 500 and 840 cm^{-1} shifted by approximately 50 cm^{-1} with respect to the corresponding experimental features. In correspondence to the two features of the ϵ_2, the ϵ_1 shows typical S-shaped resonances. The comparisons carried out in Fig. 10 imply that the vibrational modes of our model structure are sufficiently good for describing the global shape of the dielectric function. Particularly good is the agreement found for the frequency position of the main features of both ϵ_1 and ϵ_2.

The absorption spectrum $\alpha(\omega)$ and the refractive index $n(\omega)$ at a frequency ω can be obtained from the real and imaginary parts of the dielectric function:

$$\alpha(\omega) = \frac{\omega}{cn(\omega)}\epsilon_2(\omega), \quad (4)$$

$$n(\omega) = \sqrt{\frac{\epsilon_1(\omega) + \sqrt{\epsilon_1(\omega)^2 + \epsilon_2(\omega)^2}}{2}}, \quad (5)$$

where c is the speed of the light.[84] In Figs. 11(a) and 11(b) we report the refractive index and the absorption spectrum in the infrared, compared to the experimental spectra obtained for CVD silicon nitride films in Refs. 83 and 85, respectively. The refractive index is clearly reminiscent of the ϵ_1 behavior of Fig. 10, showing also a similar level of agreement with experiment. The calculated absorption spectrum

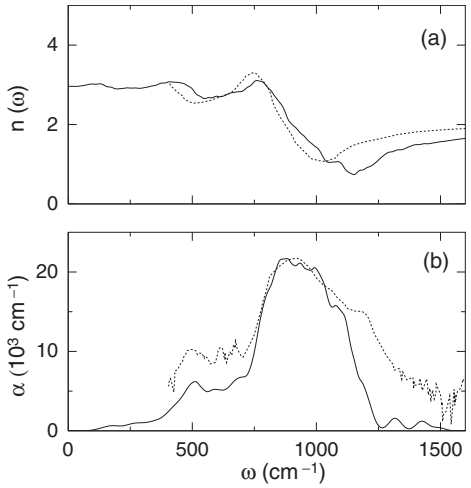

FIG. 11. (a) Calculated (solid) and experimental (dotted, Ref. 83) refraction index $n(\omega)$ of a-Si_3N_4. (b) Calculated (solid) and experimental FTIR (dotted, Ref. 85) absorption spectra of a-Si_3N_4. The experimental absorption spectrum (originally given in arbitrary units) was rescaled so that its maximum coincide with the maximum of the calculated spectrum.

fairly reproduces the main broad peak at ~900 cm^{-1} and the side peak at ~500 cm^{-1} of the experimental spectrum. These are originated by the two main peaks of the ϵ_2 which are shifted by the multiplying ω factor and by the decreasing trend of $n(\omega)$ between 770 and 1150 cm^{-1}. Although the spectrum reported in Ref. 85 is given only in arbitrary units, the maximum value of the calculated absorption spectrum is consistent with the maxima from the experimental spectra of hydrogenated amorphous silicon nitride samples in Ref. 72.

The decomposition of the nitrogen contribution to the v-DOS according to local vibrations is helpful for understanding the origin of the main infrared peaks. From the analysis shown in Fig. 8(b) we derive a picture of the vibrational modes around 500 cm^{-1} mainly arising from rocking nitrogen motions together with a fraction of silicon motions. In Ref. 7, Lucovsky *et al.* suggested that the main peak in the infrared-absorption spectrum is originated by asymmetric Si-N bond-stretching vibrations. This is supported by our analysis of the v-DOS showing that nitrogen stretching motion dominates the range 800–950 cm^{-1}. The experimental infrared-absorption spectrum reported in Fig. 11(b) features a shoulder at 1180 cm^{-1} which has been attributed to N-H bending vibrations.[7,85] Incidentally, we note that the calculated spectrum falls down abruptly above ~1100 cm^{-1} consistently with the very small concentration of H atoms in our model, and consistently with the v-DOS of Fig. 8. Furthermore, we speculate that the experimental infrared-absorption spectrum might show in the range 1200–1500 cm^{-1} features originated by stretching motions of twofold coordinated N atoms as our analysis of the v-DOS suggests [Fig. 9(b)].

VII. RAMAN SPECTRA

Raman spectra of amorphous materials are usually obtained for incoming and outgoing photons with either parallel (VV) or cross (HV) polarization configuration. The experimental VV Raman spectrum of a-Si_3N_4 in the range up to 1500 cm^{-1} is characterized by two very broad bands below and above ~600 cm^{-1}.[86,87] We note that both bands do not show any sharp feature analogous to the defect lines[88] in SiO_2 or to the boroxol peak[23] in B_2O_3. As these are originated by well localized vibrational modes, we infer that similar localized Raman active modes are not present in a-Si_3N_4.

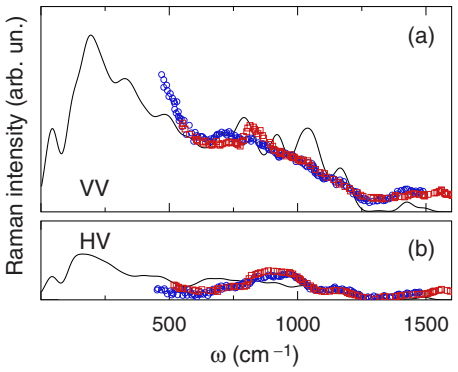

FIG. 12. (Color online) Calculated (solid) and experimental Raman spectra of a-Si_3N_4 (a) in parallel and (b) in cross polarization configurations. Experimental data for composition ratios $r=1.35$ (circles) and $r=1.4$ (squares) are taken from Ref. 86. The theoretical spectra are scaled to match the integrated intensity of the experimental spectra. A Gaussian broadening of 25 cm^{-1} is used.

In Fig. 12, we compare the VV and HV Raman spectra calculated for our model to the experimental spectra of Ref. 86. The calculated VV Raman spectrum shows a series of peaks between 750–1200 cm^{-1} that are not visible in the experiment. However the average intensity in this range appears to be in fair agreement with the experiment. As expected, the Raman intensity of the HV spectrum is found weaker than that of the VV spectrum. The difference between the theory and the experiment might be explained by the limited statistics of our model structure and in part by the limited resolution of the experiments. In Fig. 13 we report the reduced VV and HV Raman spectra where the thermal dependence has been dropped.[42] This permits a better reading of the relative intensities of the features appearing in the spectrum. In both reduced VV and HV spectra the intensity of the features at frequencies above ~600 cm^{-1} is enhanced

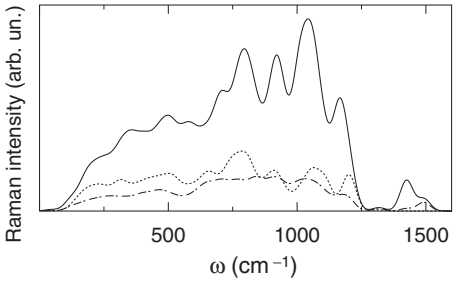

FIG. 13. Calculated reduced Raman spectra of a-Si_3N_4 in parallel (solid) and in cross (dot-dashed) polarization configuration. Contribution from two-membered rings (dotted) is also shown for parallel polarization configuration. A Gaussian broadening of 25 cm^{-1} is used.

with respect to that of the features at lower frequencies. By considering the decomposition of the v-DOS in terms of local vibrations [Fig. 8(b)], we deduce that the vibrational modes originating mainly from N stretching motions exhibit a larger Raman coupling.

As two-membered rings constitute a well identified structural unit of the a-Si_3N_4 network (Sec. III A), it is worth analyzing their behavior. Hence, we also considered the VV Raman intensity coming from two-membered rings and found that they give a contribution throughout all the spectral range of Fig. 13. Furthermore, we note that none of the peaks in the theoretical VV Raman spectrum can be attributed exclusively to vibrations in two-membered rings. Finally, hydrogen atoms are found to give rise to a strong peak at $\sim 3300\ cm^{-1}$, consistently with the analysis of the v-DOS in Fig. 9.

VIII. CONCLUSIONS

In this work we investigated the electronic, structural, and vibrational properties of a-Si_3N_4 through a first-principles spectroscopy approach. First, we focused on neutron-diffraction probes and calculated, within the harmonic approximation, the neutron total structure factor, the radial distribution, and the pair-correlation functions. Next, we calculated the quasiparticle electronic density of states through an accurate *GW* approach which permits calculations in large model structures with substantially higher accuracy with respect to ordinary density-functional calculations. Finally, we investigated vibrational properties and calculated infrared and Raman spectra by using a finite electric field approach. For the calculated spectra and the calculated physical properties we obtained a good overall agreement with the available experimental data. This supports a picture of a-Si_3N_4 displaying a considerable amount of edge-sharing SiN_4 tetrahedra. Our analysis furthermore investigates the role of point defects, which constitutes an important feature in samples used for microelectronic applications. These are found to be responsible for specific contributions to the electronic density of states and to the vibrational density of states.

The methodology applied in this work proved successful for obtaining several insights at the atomistic level into the physics of amorphous silicon nitride. Consequently, it is appropriate for investigating structural, vibrational, and electronic properties of more complex materials based on silicon nitride.

ACKNOWLEDGMENTS

We acknowledge S. Scandolo and A. Pasquarello for their helpful comments and suggestions. The calculations were performed using the computational facilities of ICTP and CINECA. This work has been partially funded under the Italian CNR-INFM *Seed Projects* scheme.

[1] R. N. Katz, Science **208**, 841 (1980); A. Y. Liu and M. L. Cohen, Phys. Rev. B **41**, 10727 (1990).
[2] Y. Ma, T. Yasuda, and G. Lucovsky, Appl. Phys. Lett. **64**, 2226 (1994).
[3] H. Aozasa, I. F. Ujiwara, A. Nakamura, and Y. Komatsu, Jpn. J. Appl. Phys. **38**, 1441 (1999); H. Bachhofer, H. Reisinger, E. Bertagnolli, and H. von Philipsborn, J. Appl. Phys. **89**, 2791 (2001).
[4] L. Dal Negro, S. Hamel, N. Zaitseva, J. H. Yi, A. Williamson, M. Stolfi, J. Michel, G. Galli, and L. C. Kimerling, IEEE J. Sel. Top. Quantum Electron. **12**, 1151 (2006); L. Dal Negro, J. H. Yi, J. Michel, L. C. Kimerling, S. Hamel, A. Williamson, and G. Galli, *ibid.* **12**, 1628 (2006); L. Dal Negro, J. H. Yi, L. C. Kimerling, S. Hamel, A. Williamson, and G. Galli, Appl. Phys. Lett. **88**, 183103 (2006).
[5] H. O. Pierson, *Handbook of Chemical Vapor Deposition* (Noyes Publications, Norwich, NY, 1999).
[6] D. M. Mattox, *Handbook of Physical Vapor Deposition (PVD) Processing* (Noyes Publications, Westwood, NJ, 1998).
[7] G. Lucovsky, J. Yang, S. S. Chao, J. E. Tyler, and W. Czubatyj, Phys. Rev. B **28**, 3234 (1983); D. V. Tsu, G. Lucovsky, and M. J. Mantini, *ibid.* **33**, 7069 (1986).
[8] V. Verlaan, C. H. M. van der Werf, W. M. Arnoldbik, H. D. Goldbach, and R. E. I. Schropp, Phys. Rev. B **73**, 195333 (2006).
[9] K.-C. Lin and S.-C. Lee, J. Appl. Phys. **72**, 5474 (1992).
[10] S. M. Hu, J. Electrochem. Soc. **113**, 693 (1966); M. F. Lambrinos, R. Valizadeh, and J. S. Colligon, Appl. Opt. **35**, 3620 (1996); G. Claudio, S. Calnan, K. Bass, and M. Boreland, J. Mater. Sci.: Mater. Electron. **19**, 285 (2008).
[11] P. Kroll, J. Non-Cryst. Solids **293-295**, 238 (2001).
[12] M. Misawa, T. Fukunaga, K. Niihara, T. Hirai, and K. Suzuki, J. Non-Cryst. Solids **34**, 313 (1979).
[13] T. Aiyama, T. Fukunaga, K. Niihara, T. Hirai, and K. Suzuki, J. Non-Cryst. Solids **33**, 131 (1979).
[14] L. Giacomazzi, P. Umari, and A. Pasquarello, Phys. Rev. B **79**, 064202 (2009).
[15] A. Pasquarello and R. Car, Phys. Rev. Lett. **79**, 1766 (1997).
[16] A. Pasquarello and R. Car, Phys. Rev. Lett. **80**, 5145 (1998).
[17] L. Giacomazzi, P. Umari, and A. Pasquarello, Phys. Rev. B **74**, 155208 (2006).
[18] P. Umari and A. Pasquarello, Phys. Rev. Lett. **89**, 157602 (2002); I. Souza, J. Íñiguez, and D. Vanderbilt, *ibid.* **89**, 117602 (2002).
[19] See, e.g., R. M. Martin, *Electronic Structure* (Cambridge University Press, Cambridge, 2004) and references quoted therein.
[20] G. Onida, L. Reining, and A. Rubio, Rev. Mod. Phys. **74**, 601 (2002).
[21] L. Giacomazzi, C. Massobrio, and A. Pasquarello, Phys. Rev. B **75**, 174207 (2007).
[22] L. Giacomazzi, P. Umari, and A. Pasquarello, Phys. Rev. Lett. **95**, 075505 (2005).
[23] P. Umari and A. Pasquarello, Phys. Rev. Lett. **95**, 137401 (2005).

[24] F. de Brito Mota, J. F. Justo, and A. Fazzio, Phys. Rev. B **58**, 8323 (1998).
[25] L. Ouyang and W. Y. Ching, Phys. Rev. B **54**, R15594 (1996).
[26] M. Gastreich, J. D. Gale, and C. M. Marian, Phys. Rev. B **68**, 094110 (2003); S. R. Billeter, A. Curioni, D. Fischer, and W. Andreoni, *ibid.* **73**, 155329 (2006).
[27] P. Vashishta, R. K. Kalia, and I. Ebbsjö, Phys. Rev. Lett. **75**, 858 (1995).
[28] F. Alvarez and A. A. Valladares, Appl. Phys. Lett. **80**, 58 (2002); F. Alvarez, C. C. Díaz, A. A. Valladares, and R. M. Valladares, Phys. Rev. B **65**, 113108 (2002).
[29] F. Alvarez and A. A. Valladares, Phys. Rev. B **68**, 205203 (2003).
[30] J. F. Justo, F. de Brito Mota, and A. Fazzio, Phys. Rev. B **65**, 073202 (2002); F. de Brito Mota, J. F. Justo, and A. Fazzio, Braz. J. Phys. **32**, 436 (2002).
[31] G. Pacchioni and D. Erbetta, Phys. Rev. B **60**, 12617 (1999); **61**, 15005 (2000).
[32] L. Hedin, Phys. Rev. **139**, A796 (1965).
[33] F. Aryasetiawan and O. Gunnarsson, Rep. Prog. Phys. **61**, 237 (1998).
[34] M. S. Hybertsen and S. G. Louie, Phys. Rev. Lett. **55**, 1418 (1985).
[35] L. Hedin and S. Lundqvist, Solid State Phys. **23**, 1 (1970).
[36] R. Car and M. Parrinello, Phys. Rev. Lett. **55**, 2471 (1985).
[37] A. Pasquarello, K. Laasonen, R. Car, C. Y. Lee, and D. Vanderbilt, Phys. Rev. Lett. **69**, 1982 (1992); K. Laasonen, A. Pasquarello, R. Car, C. Y. Lee, and D. Vanderbilt, Phys. Rev. B **47**, 10142 (1993).
[38] http://www.quantum-espresso.org
[39] J. P. Perdew and A. Zunger, Phys. Rev. B **23**, 5048 (1981).
[40] D. Vanderbilt, Phys. Rev. B **41**, 7892 (1990).
[41] P. Umari, G. Stenuit, and S. Baroni, Phys. Rev. B **79**, 201104(R) (2009).
[42] P. Umari and A. Pasquarello, Diamond Relat. Mater. **14**, 1255 (2005).
[43] S. M. Sze, *Physics of Semiconductor Devices* (Wiley and Sons, New York, 1981).
[44] In simulations of silica performed at constant pressure [K. Vollmayr, W. Kob, and K. Binder, Phys. Rev. B **54**, 15808 (1996)], it was shown that quenching from the melt gives glass structures whose densities depend on the quenching rate. As *ab initio* quenching rates are too large for achieving a converged density, we preferred to fix the density at the experimental value of Ref. 43.
[45] S. Nosé, Mol. Phys. **52**, 255 (1984); W. G. Hoover, Phys. Rev. A **31**, 1695 (1985).
[46] We successively observed that the passivated empty state actually is spatially localized close to a twofold coordinated nitrogen atom, in accord with the experimental assignments of Ref. 47.
[47] W. L. Warren, P. M. Lenahan, and S. E. Curry, Phys. Rev. Lett. **65**, 207 (1990); P. M. Lenahan and S. E. Curry, Appl. Phys. Lett. **56**, 157 (1990); W. L. Warren, J. Kanicki, J. Robertson, and P. M. Lenahan, *ibid.* **59**, 1699 (1991).
[48] *Properties of Amorphous Silicon and its Alloys*, edited by T. Searle (INSPEC, London, 1998); V. A. Gritsenko, Y. N. Novikov, A. V. Shaposhnikov, H. Wong, G. M. Zhidomirov, Phys. Solid State **45**, 2031 (2003).
[49] J. F. Stebbins, Nature (London) **351**, 638 (1991); R. E. Youngman and S. Sen, J. Non-Cryst. Solids **337**, 182 (2004).
[50] G. Pacchioni, F. Frigoli, D. Ricci, and J. A. Weil, Phys. Rev. B **63**, 054102 (2000); J. Laegsgaard and K. Stokbro, Phys. Rev. Lett. **86**, 2834 (2001).
[51] S. Sicolo, G. Palma, C. Di Valentin, and G. Pacchioni, Phys. Rev. B **76**, 075121 (2007).
[52] M. d'Avezac, M. Calandra, and F. Mauri, Phys. Rev. B **71**, 205210 (2005); M. F. Camellone, T. D. Kühne, and D. Passerone, Phys. Rev. B **80**, 033203 (2009).
[53] M. Stengel and N. A. Spaldin, Phys. Rev. B **77**, 155106 (2008).
[54] A. A. Bagatur'yants, K. P. Novoselov, A. A. Safonov, J. Vernon Cole, M. Stoker, and A. A. Korkin, Surf. Sci. **486**, 213 (2001).
[55] R. Jones, S. Öberg, F. Berg Rasmussen, and B. Bech Nielsen, Phys. Rev. Lett. **72**, 1882 (1994).
[56] C. E. Jesurum, V. Pulim, and L. W. Hobbs, J. Nucl. Mater. **253**, 87 (1998).
[57] A. Zerr, G. Miehe, G. Serghioum, M. Schwarz, E. Kroke, R. Riedel, H. Fuess, P. Kroll, and R. Boehler, Nature (London) **400**, 340 (1999).
[58] Neutron-scattering lengths and cross sections are taken from http://www.ncnr.nist.gov/resources/n-lengths/
[59] A. Pasquarello, Phys. Rev. B **61**, 3951 (2000).
[60] S. Scandolo, P. Giannozzi, C. Cavazzoni, S. de Gironcoli, A. Pasquarello, and S. Baroni, Z. Kristallogr. **220**, 574 (2005).
[61] N. Binggeli, N. Troullier, J. L. Martins, and J. R. Chelikowsky, Phys. Rev. B **44**, 4771 (1991); F. Giustino and A. Pasquarello, Phys. Rev. Lett. **96**, 216403 (2006).
[62] F. Alvarez and A. A. Valladares, Rev. Mex. Fis. **48**, 528 (2002).
[63] A. N. Sorokin, A. A. Karpushin, V. A. Gritsenko, and H. Wong, J. Non-Cryst. Solids **354**, 1531 (2008).
[64] R. Kärcher, L. Ley, and R. L. Johnson, Phys. Rev. B **30**, 1896 (1984).
[65] L. Martín-Moreno, E. Martínez, J. A. Vergés, and F. Yndurain, Phys. Rev. B **35**, 9683 (1987); S.-Y. Lin, Opt. Mater. (Amsterdam, Neth.) **23**, 93 (2003).
[66] J. Bauer, Phys. Status Solidi **39**, 411 (1977).
[67] S. R. Elliott, *Physics of Amorphous Materials* (Longman, New York, 1984), p. 194.
[68] C.-K. Loong, P. Vashishta, R. K. Kalia, and I. Ebbsjö, Europhys. Lett. **31**, 201 (1995).
[69] A. Omeltchenko, A. Nakano, R. K. Kalia, and P. Vashishta, Europhys. Lett. **33**, 667 (1996).
[70] R. J. Bell, P. Dean, and D. C. Hibbins-Butler, J. Phys. C **4**, 1214 (1971); A. Pasquarello, J. Sarnthein, and R. Car, Phys. Rev. B **57**, 14133 (1998); S. N. Taraskin and S. R. Elliott, *ibid.* **56**, 8605 (1997).
[71] A. Kuwabara, K. Matsunaga, and I. Tanaka, Phys. Rev. B **78**, 064104 (2008).
[72] Z. Yin and F. W. Smith, Phys. Rev. B **42**, 3666 (1990).
[73] F. Giustino and A. Pasquarello, Phys. Rev. Lett. **95**, 187402 (2005).
[74] N. Zotov, M. Marinov, N. Mousseau, and G. Barkema, J. Phys.: Condens. Matter **11**, 9647 (1999).
[75] R. Biswas, A. M. Bouchard, W. A. Kamitakahara, G. S. Grest, and C. M. Soukoulis, Phys. Rev. Lett. **60**, 2280 (1988).
[76] R. Resta, Rev. Mod. Phys. **66**, 899 (1994).
[77] Y. Cai, L. Zhang, Q. Zeng, L. Cheng, and Y. Xu, Phys. Rev. B **74**, 174301 (2006).
[78] The average was carried out in the supercell reference system.
[79] A. Pasquarello and R. Resta, Phys. Rev. B **68**, 174302 (2003).
[80] H. R. Philipp, in *Handbook of Optical Constants of Solids*,

edited by D. Palik (Academic Press, San Diego, 1998), p. 774; E. Dehan, P. Temple-Boyer, R. Henda, J. J. Pedroviejo, and E. Scheid, Thin Solid Films **266**, 14 (1995).

[81] *Handbook of Semiconductor Manufacturing Technology*, 2nd ed., edited by R. Doering and Y. Nishi (CRC Press, Boca Raton, FL, 2007), p. 325.

[82] G. N. Parsons, J. H. Souk, and J. Batey, J. Appl. Phys. **70**, 1553 (1991).

[83] M. Klanjšek Gunde and M. Maček, Phys. Status Solidi A **183**, 439 (2001).

[84] H. Kuzmany, *Solid-State Spectroscopy* (Springer-Verlag, Berlin, 1998).

[85] R. K. Pandey, L. S. Patil, J. P. Bange, and D. K. Gautam, Opt. Mater. (Amsterdam, Neth.) **27**, 139 (2004).

[86] J. Bandet, B. Despax, and M. Caumont, J. Appl. Phys. **85**, 7899 (1999).

[87] N. Wada, S. A. Solin, J. Wong, and S. Prochazka, J. Non-Cryst. Solids **43**, 7 (1981).

[88] F. L. Galeener and G. Lucovsky, Phys. Rev. Lett. **37**, 1474 (1976); F. L. Galeener, Solid State Commun. **44**, 1037 (1982).